

Facile reconstruction of time-resolved fluorescence data with exponentially modified Gaussians

Darien J. Morrow¹ and Xuedan Ma^{1,2,3,*}

¹Center for Nanoscale Materials, Argonne National Laboratory, Lemont, Illinois 60439, United States

²Consortium for Advanced Science and Engineering,
University of Chicago, Chicago, Illinois 60637, United States

³Northwestern-Argonne Institute of Science and Engineering, 2205 Tech Drive, Evanston, IL 60208, USA

(Dated: January 12, 2022)

Analyte response is convoluted with instrument response in time resolved fluorescence data. Decoding the desired analyte information from the measurement usually requires tedious, iterative numerical convolutions. Here in, we show that time resolved data can be completely reconstructed without numerical convolutions. Our strategy relies on a summation of exponentially modified Gaussians which encode all convolutions within easily evaluated complementary error functions.

I. INTRODUCTION

Time resolved fluorescence is a ubiquitous measurement used in fields as diverse as materials physics,[1] physical chemistry,[2] structural biology,[3, 4] robotic surgery,[5] and art conservation.[6] In these uses, the metric of interest is the set of fluorescence lifetimes, $\{\tau_i\}$, which is defined by the physical identity and structure of the sample. In the Platonic ideal of the experiment, a sample is excited with an infinitely fast pulse of light, the sample then undergoes spontaneous emission with first order kinetics, so the emitted intensity of light decays exponentially with time. The emitted light is finally measured with an infinitely fast detector. In actuality, excitation pulses have finite width and detectors have finite response times (Figure 1). These non-idealities must be accounted for in data analysis routines to extract useful and representative fluorescence lifetimes.

If S is the ideal signal, the measured response, M , is the convolution of the ideal signal with some instrument response function, R , which accounts for the non-idealities of reality,

$$M = S * R. \quad (1)$$

Deconvolution of S from M can be accomplished if R is exactly known. If R is not known with certainty, then deconvolution is a non-convex (usually unfeasible) optimization problem. Instead most commercial software packages and individual researchers rely on a reconvolution strategy in which a decay model, S_{model} , is convolved with a measured (or supposed) instrument response function, R_{measured} ,

$$M_{\text{model}} = S_{\text{model}} * R_{\text{measured}}. \quad (2)$$

The resultant signal, M_{model} , is compared to M . The parameters which define S_{model} are then iteratively adjusted to minimize the difference between M_{model} and M

in order to extract a representation of S . In the case of methods like Fluorescence Lifetime Imaging (FLIM), the extraction of S must then be accomplished for thousands of time traces which each represents a pixel of a spatial map.[7]

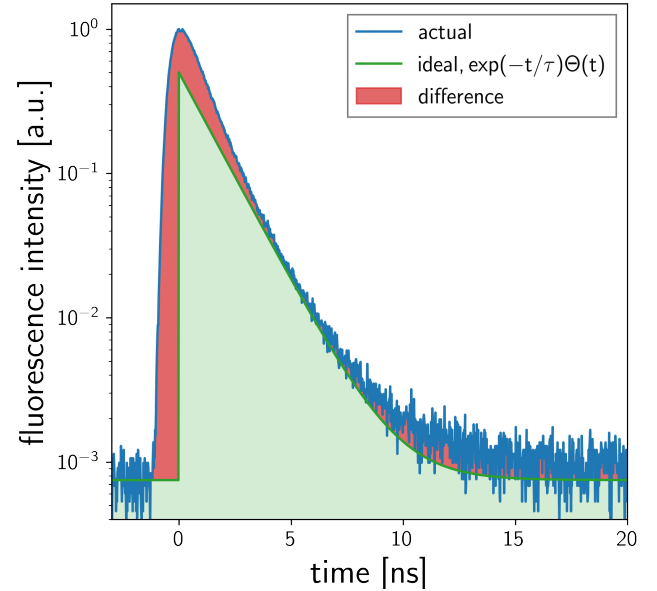


FIG. 1. Actual time-resolved fluorescence data, M , versus the ideal exponential decay predicted from first order kinetics, S . $\tau = 1/\lambda = 1.5$ ns.

The reconvolution strategy is usually robust and generates an accurate view of the dynamics encoded in fluorescence data. In practice, it can be difficult to correctly zero-pad and interpolate S_{model} and R . Moreover, if one does not use an easily scriptable analysis software, then one must iterate the parameters defining S_{model} manually, which can be time consuming. Closed source commercial software packages (e.g. SPCImage NG from Becker & Hickl and EasyTau 2 from Picoquant) and open source packages (e.g. DecayFit and FLIMfit,[8]) exist to help solve the problems associated with fitting fluorescence data to extract lifetimes via numerical con-

* xuedan.ma@anl.gov

volution. Without using these packages, in many cases, researchers choose to assume the mid to late time dynamics encoded in their datasets are representative of S and therefore just fit S_{model} to $M(t > t_{\text{cutoff}})$, which is a good assumption in some limits. It is likely that this choice is oftentimes made not for suitability of assumption, but instead because it can be hard to correctly implement numerical convolutions.

Herein we introduce an analytic solution to this numerical convolution problem. We derive an integral equation which accounts for any number of exponential decay processes in both the sample response and instrument response. All numerically difficult convolutions are accounted for analytically. Our result is constructed so that analysis of time-resolved fluorescence data exclusively uses the robust algorithms which are packaged in most software packages to calculate the values of exponential and error functions. We demonstrate the utility of our result for reconstructing the wavelength dependent response of a commercial single-photon avalanche diode (SPAD) and also for retrieving the decay lifetimes of a model system.

II. DERIVATION OF PRIMARY RESULT

In this section we derive our primary result (Equation 27).

A. Exponentially modified Gaussian: $h(x)$

We start by assuming that fluorescence decay processes can be described using monoexponential decays

$$f(x; \lambda) \equiv \lambda \exp[-\lambda x] \Theta[x], \quad (3)$$

$$\Theta[x] \equiv \begin{cases} 1, & x > 0 \\ 0, & x \leq 0 \end{cases}. \quad (4)$$

in which Θ is the Heaviside step function, which accounts for the sample not emitting until after it is excited. The lifetime of a component is given by $\tau_i = \frac{1}{\lambda_i}$. The ideal instrument response function (IRF) is considered to be a Gaussian

$$g(x; \mu, \sigma) \equiv \frac{1}{\sigma\sqrt{2\pi}} \exp\left[-\left(\frac{x-\mu}{\sqrt{2}\sigma}\right)^2\right], \quad (5)$$

with σ characterizing the temporal width and μ defining the ‘‘time zero’’ of the instrument. Later we will account for non-Gaussian IRFs. Note that, for clarity, $f(x)$ and $g(x)$ are both written as normalized functions so that $\int_{-\infty}^{\infty} f(x)dx = 1$ —this choice does not affect the form of our final result.

We now define a composite function which will be the

mainstay of our derivation,

$$h(x; \mu, \sigma, \lambda) \equiv f(x; \lambda) * g(x; \mu, \sigma), \quad (6)$$

$$(f * g)(t) \equiv \int_{-\infty}^{\infty} f(\tau)g(t - \tau)d\tau. \quad (7)$$

Here, $*$ is the convolution operator which, importantly, is commutative, associative, and distributive. In Appendix A we show that h is a function known as the *exponentially modified Gaussian* (EMG) with form,

$$h(x; \mu, \sigma, \lambda) = \frac{\lambda}{2} \exp\left[\frac{\lambda}{2}(2\mu + \lambda\sigma^2 - 2x)\right] \times \text{erfc}\left[\frac{\mu + \lambda\sigma^2 - x}{\sqrt{2}\sigma}\right], \quad (8)$$

where

$$\text{erfc}(t) \equiv 1 - \text{erf}(t) = \frac{2}{\sqrt{\pi}} \int_t^{\infty} \exp[-\tau^2]d\tau. \quad (9)$$

In Equation 8, the convolution operation present in Equation 6 is rewritten as a single *complementary error* function. The EMG is commonly used in many fields as a phenomenological quantification tool: in the chromatography and mass spectrometry fields it is used to quantify tailed lineshapes,[9–11] in psychophysiology it is used to quantify response times,[12, 13] and in material science it has seen limited use fitting fluorescence spectra and diffusion profiles from inhomogeneous semiconductors.[14–18]

Figure 2a graphs f , g , and h . At early times h is similar to the Gaussian IRF, g , but at late times, h follows the exponential decay, f . Figure 2 validates the intuition that if the dynamics of interest are much longer than the width of the IRF, then one can extract the lifetimes of interest by fitting the long-time tail of the measured response. Figure 2b shows how larger widths of the IRF (σ) pushes the peak maximum of h to later times.

B. Extension of $h(x)$ with multiple decay functions

For multiple decay pathways we write a distribution of exponential decays,

$$F^{(i)}(x) \equiv \sum_i^m a_i \lambda_i \exp[-\lambda_i x] \Theta[x] \quad (10)$$

$$= \sum_i^m f_i(x), \quad (11)$$

with a_i being a weighting factor for each exponential decay with $\alpha_i \equiv a_i \lambda_i$ being the unnormalized weight. Convolution of this distribution of decays with a Gaussian yields

$$H^{(i)}(x) \equiv g(x) * F^{(i)}(x) \quad (12)$$

$$= \sum_i^m g(x) * f_i(x) \quad (13)$$

$$= \sum_i^m a_i h_i(x) \quad (14)$$

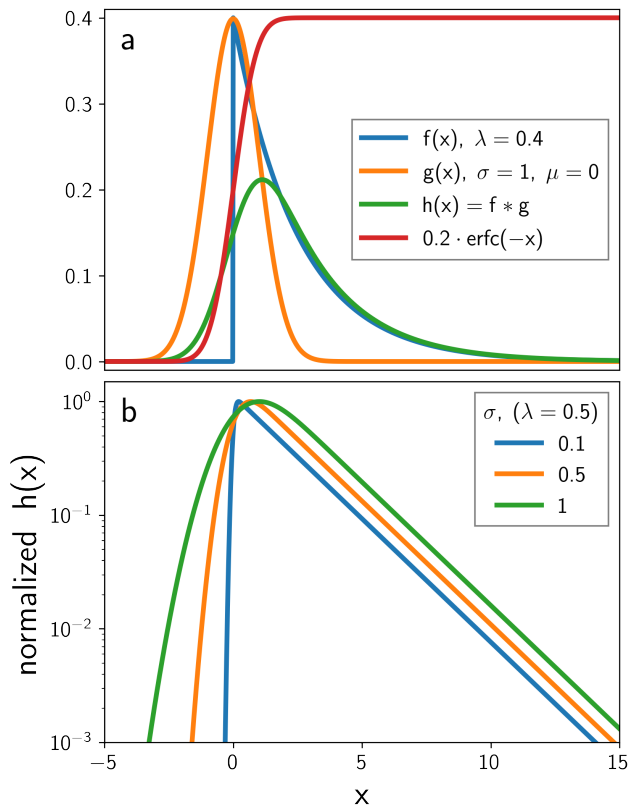


FIG. 2. Graphical form of the exponentially modified Gaussian. (a) Graph of Equation 3, Equation 5, and Equation 6 for $\lambda = 0.4$, $\sigma = 1$ and $\mu = 0$. A scaled form of Equation 9 is also shown to highlight its sigmoid-like behavior. (b) Equation 6 with $\lambda = 0.5$ and $\sigma \in \{0.1, 0.5, 1\}$ showing how larger values of σ decreases the angle of h at negative x and pushes the maximum to positive x .

in which we noted that convolution is a linear operation and therefore distributive. Here we emphasize that $h_i(x) = h(x; \mu, \sigma, \lambda_i)$ which means that there are single μ and σ but multiple λ_i . If a time-resolved fluorescence experiment has a Gaussian IRF, then $H^{(i)}(x)$ describes the measured response of a sample with a set, $\{\lambda_i\}$, of decay pathways.

C. Detectors with non-Gaussian, tailed IRFs

Oftentimes SPAD detectors do *not* have Gaussian IRFs, but instead have a long tail towards positive times. Phenomenologically these non-ideal IRFs may be described with a distribution of weights and rates. In this case we interpret $H^{(i)}(x)$ as the IRF. We then account for analyte response by convolving $H^{(i)}(x)$ (our IRF) with a second $F^{(j)}(x)$ (the true sample decay pathways) to form a representative measured signal, \mathcal{M} ,

$$\mathcal{M}(x) = H^{(i)}(x) * F^{(j)}(x), \quad (15)$$

which may be rewritten as

$$\mathcal{M}(x) = g(x) * F^{(i)}(x) * F^{(j)}(x) \quad (16)$$

$$= g(x) * \left\{ \sum_i^m f_i(x) \right\} * \left\{ \sum_j^n f_j(x) \right\} \quad (17)$$

$$= g(x) * \left\{ \sum_{i,j}^{m,n} f_i(x) * f_j(x) \right\} \quad (18)$$

$$= g(x) * \left\{ \sum_{i,j}^{m,n} y_{i,j}(x) \right\}. \quad (19)$$

To solve the double convolution present in Equation 19 we first consider the argument of the summand inside the braces

$$y_{i,j}(t) = f_i(t) * f_j(t) \quad (20)$$

$$= a_i \lambda_i a_j \lambda_j \int_{-\infty}^{\infty} e^{-\lambda_i \tau} \Theta[\tau] e^{-\lambda_j(t-\tau)} \Theta[t-\tau] d\tau. \quad (21)$$

This integrand is nonzero only when $\tau > 0$ and $t - \tau > 0$ so

$$y_{i,j}(t) = a_i \lambda_i a_j \lambda_j \exp[-\lambda_j t] \Theta[t] \int_0^t \exp[\tau(\lambda_j - \lambda_i)] d\tau \quad (22)$$

$$= \left(\frac{a_j \lambda_j}{\lambda_j - \lambda_i} \right) f_i(t) + \left(\frac{a_i \lambda_i}{\lambda_i - \lambda_j} \right) f_j(t) \quad (23)$$

in which we noted the standard integral

$$\int_0^t \exp[\tau(\lambda_j - \lambda_i)] d\tau = \frac{1 - \exp[(\lambda_j - \lambda_i)t]}{\lambda_j - \lambda_i} \quad (24)$$

which is only true when $\lambda_j \neq \lambda_i$. Substitution of $y_{i,j}$ from Equation 23 into Equation 19 yields our measured response

$$\mathcal{M}(x) = g(x) * \sum_{i,j}^{m,n} \left\{ \left(\frac{a_j \lambda_j}{\lambda_j - \lambda_i} \right) f_i(x) + \left(\frac{a_i \lambda_i}{\lambda_i - \lambda_j} \right) f_j(x) \right\}, \quad (25)$$

$$= \sum_{i,j}^{m,n} \left\{ \left(\frac{a_j \lambda_j}{\lambda_j - \lambda_i} \right) h_i(x) + \left(\frac{a_i \lambda_i}{\lambda_i - \lambda_j} \right) h_j(x) \right\}, \quad (26)$$

$$= \sum_i^m h_i(x) \sum_j^n \frac{a_j \lambda_j}{\lambda_j - \lambda_i} + \sum_j^n h_j(x) \sum_i^m \frac{a_i \lambda_i}{\lambda_i - \lambda_j}. \quad (27)$$

Equation 27 is our primary analytic result. It encodes the dynamics of an experiment whose IRF has an arbitrarily large number of exponential tails, and whose sample response also has an arbitrarily large number of monoexponential decays. Importantly, there are no

explicit convolutions present in Equation 27. Instead, Equation 27 requires evaluation of complementary error functions; software libraries as diverse as Microsoft Excel and the Scientific Python stack provide this capability using efficient, accurate algorithms.[19, 20] Appendix B shows two specific cases of Equation 27 with the nested summations worked out.

III. COMPARISON TO EXPERIMENTAL RESULTS

We demonstrate the utility and suitability of our strategy of exponentially modified Gaussians for time-resolved fluorescence in two case studies.

A. Fitting wavelength dependent IRF

In the first study, we characterize the instrument response of a commercial SPAD (PDM from Micro Photon Devices) and counting electronics (PicoQuant HydraHarp 400) by excitation with what is effectively a Dirac delta impulse. We couple the attenuated output of an ultrafast tuneable Ti:sapphire laser (Coherent Chameleon Discovery with Harmonics Generator, ~ 100 fs pulse width, 80 MHz repetition rate) into the SPAD. By tuning the ultrafast laser from 500 to 1075 nm and keeping SPAD count rates constant, we recover the wavelength dependent response of the SPAD and associated electronics.

Figure 3 shows that as one excites a SPAD with higher wavelength light, the response becomes longer.[21] The IRF is easily modeled with $H^{(i)}(x)$ (Equation 14)—three exponential decays are required for stellar recapitulation of the measurement. The intensity weighted average decay time,[22]

$$\tau_{\text{avg}} = \frac{\sum_i \frac{\alpha_i}{\lambda_i^2}}{\sum_i \frac{\alpha_i}{\lambda_i}}, \quad (28)$$

codifies the observation of longer instrument response times for longer wavelength excitation.

B. Fitting wavelength dependent POPOP fluorescence

In the second study, we characterize the response of powdered POPOP; 1,4-Bis(5-phenyl-2-oxazolyl)benzene; whose chemical structure is shown in Figure 4a. POPOP is a scintillator with an absorption onset in the UV-A and bright fluorescence across the visible. With an objective we focus the output of a 375 nm pulsed picosecond diode laser (Picoquant, 20 MHz repetition rate) onto powdered POPOP. Fluorescence is collected with the same objective, filtered with a 425, 525, or 610 nm

bandpass filter, and focused into a photon counting module (PerkinElmer, PicoQuant HydraHarp 400 electronics). Figure 4b shows a fluorescence spectrum of POPOP and the throughput of the three bandpass filters used.

We first measure the response function of the detector at 375 nm (Figure 4a). This IRF is fit in the same way as the IRFs in Figure 3a. Next, we measure the fluorescence of POPOP over three wavelength bands. Finally, we use our primary result, Equation 27, to fit each time trace (tri-exponential) while holding the IRF parameters constant. We recover average lifetimes of 1.1, 2.2, and 3.6 ns for the 425, 525, and 610 nm bandpass filters, respectively. The model fits all aspects of the time-resolved fluorescence exceedingly well.

IV. DISCUSSION AND CONCLUSIONS

In this work, we derived expressions for fitting the complete transient of time-resolved fluorescence measurements without requiring the use of numerical convolutions. We showed that our expressions well reproduce the tailed instrument response of a SPAD. We then showed that the SPAD IRF could be held constant while a second expression was fit to sample fluorescence. Our results suggest a clear workflow:

1. Measure instrument response and fit to

$$H^{(i)}(x; \mu, \sigma, \{a_i\}, \{\lambda_i\}) = \sum_i^m a_i h_i(x)$$

using the minimum number of exponential terms to recapitulate the measured response.

2. Measure sample response and fit to

$$\mathcal{M}(x; \{a_j\}, \{\lambda_j\}) = \sum_{i,j}^{m,n} \left(\frac{a_j \lambda_j h_i(t)}{\lambda_j - \lambda_i} + \frac{a_i \lambda_i h_j(t)}{\lambda_i - \lambda_j} \right)$$

using the minimum number of exponential terms to recapitulate the measured response while holding the IRF parameters constant.

Crucially, this workflow reconstructs the *entire* measured temporal response with no convolutions required.

While it seems to be robust, there are specific cases where this method should not be applied. First, if the material has dynamics which last longer than the period between excitation pulses then there will be some steady-state population which is not accounted for in our model. Second, if the material has kinetics which are not collectively well described by first order rate laws, then the assumption of exponential decay is poor. In both of these cases, a more holistic treatment of the fluorescence is needed, indeed there are software packages which can numerically solve the set of pulsed rate equation necessary to correctly describe the system.[23, 24] Finally, some SPADs are known to exhibit non-ideal behaviors like “afterpulsing” which can lead to IRFs which have a train of humps on the tail (note that in Figure 3a

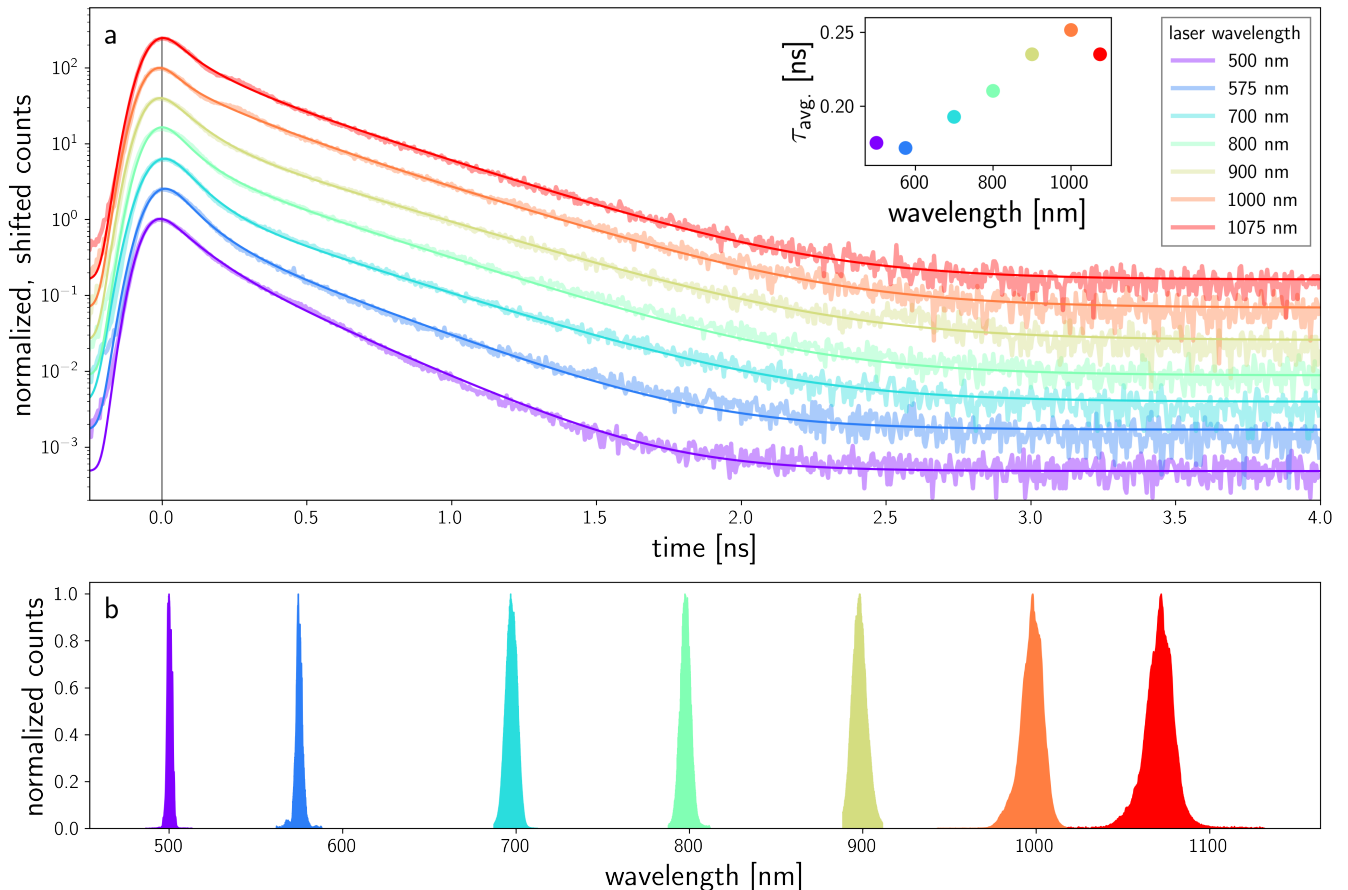


FIG. 3. Wavelength dependent SPAD IRF. (a) Temporal response from 500 to 1075 nm with thin, solid lines being the model, $H^{(i)}(x)$. Pulse profile of excitation laser is shown as gray (note how it is effectively a delta function on the nanosecond scale). Inset shows the intensity weighted average (Equation 28) of the three decay rates fit to the IRFs. (b) Color coded spectra of laser used to excite SPAD.

slight afterpulsing is present around 0.2 ns).[25, 26] If a detector's IRF is not well described by a collection of exponentially modified Gaussians which share the same width and center, then our treatment is not adequate. Instead, the linearity of convolutions allows one to have multiple weighted, and shifted ($\{\mu_k\}$) versions of the IRF which results in a third summation over μ_k . However, this level of nested summations is likely excessive and the researcher should instead accomplish convolutions with their measured, afterpulse-ridden IRF.

ACKNOWLEDGMENTS

This work was performed at the Center for Nanoscale Materials, a U.S. Department of Energy Office of Science User Facility, and supported by the U.S. Department of Energy, Office of Science, under Contract No. DE-AC02-06CH11357.

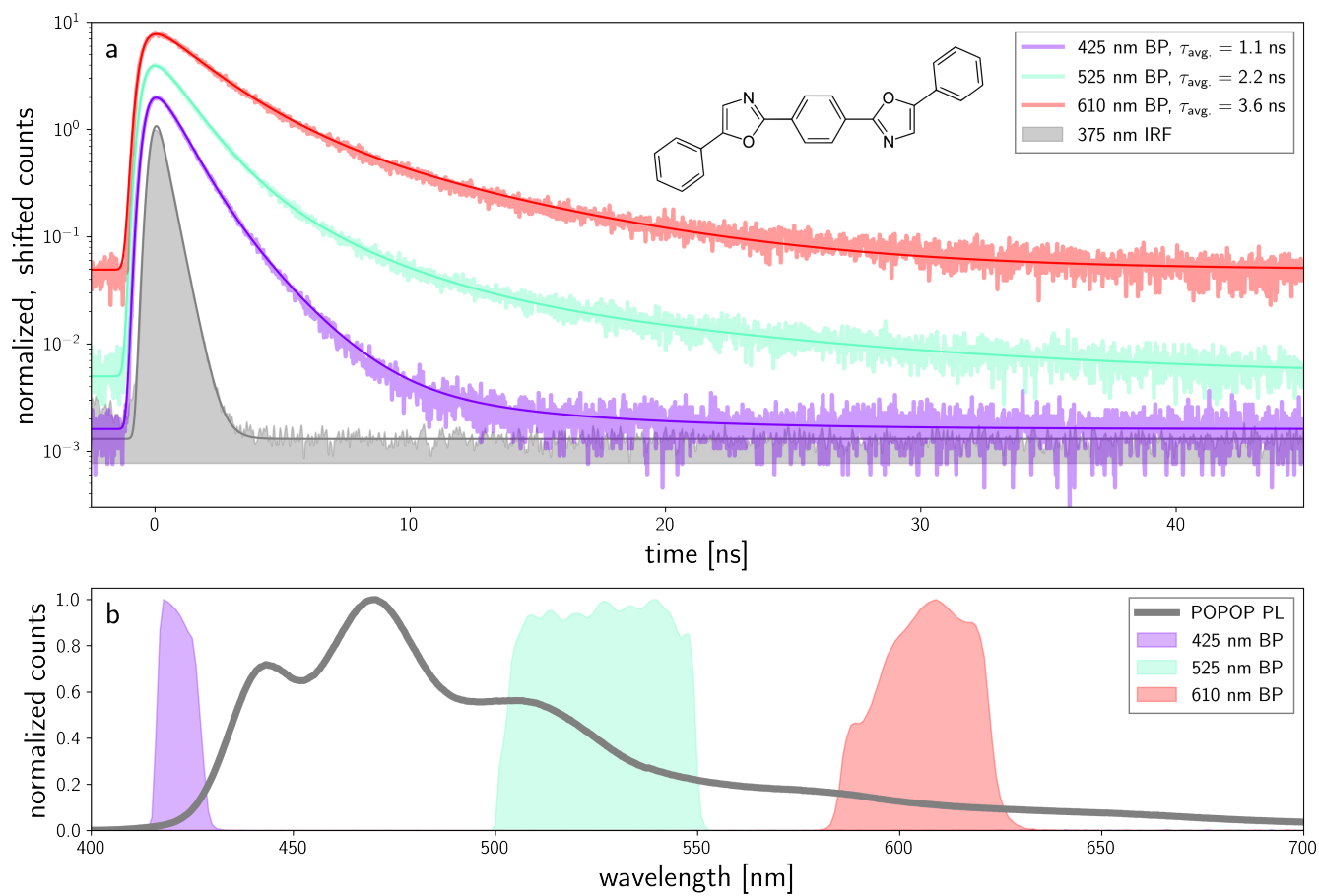


FIG. 4. Fluorescence of POPOP excited with a 375 nm pulsed didode laser. Note that the spectrum in (b) is not corrected for the wavelength dependent efficiency of our camera and collection optics.

Appendix A: Showing $h(x)$ to be an EMG

To rewrite h in a form which does not require one to perform numerical convolutions, we must cast the convolution into a complementary error function. We first write out the convolution integral in full

$$h(x; \mu, \sigma, \lambda) \equiv f(x; \lambda) * g(x; \mu, \sigma), \quad (\text{A1})$$

$$= \{\lambda \exp[-\lambda x] \Theta[x]\} * \left\{ \frac{1}{\sigma\sqrt{2\pi}} \exp\left[-\left(\frac{x-\mu}{\sqrt{2}\sigma}\right)^2\right] \right\}, \quad (\text{A2})$$

$$= \frac{\lambda}{\sigma\sqrt{2\pi}} \int_{-\infty}^{\infty} \exp[-\lambda t] \Theta[t] \exp\left[-\left(\frac{x-t-\mu}{\sqrt{2}\sigma}\right)^2\right] dt. \quad (\text{A3})$$

Because of the step function, the integrand is non-zero only when $t > 0$ so we can rewrite the bounds of integration

$$h(x; \mu, \sigma, \lambda) = \frac{\lambda}{\sigma\sqrt{2\pi}} \int_0^{\infty} \exp[-\lambda t] \exp\left[-\left(\frac{x-t-\mu}{\sqrt{2}\sigma}\right)^2\right] dt. \quad (\text{A4})$$

We will perform this integration by substitution. We define a new variable, u ,

$$u \equiv \frac{\mu + \lambda\sigma^2 - x + t}{\sqrt{2}\sigma} \quad (\text{A5})$$

$$\implies du = \frac{dt}{\sqrt{2}\sigma} \quad (\text{A6})$$

$$\implies t = \sqrt{2}\sigma u - \mu - \lambda\sigma^2 + x \quad (\text{A7})$$

Proper substitution of u into Equation A4 yields

$$h(x; \mu, \sigma, \lambda) = \frac{\sqrt{2}\sigma\lambda}{\sigma\sqrt{2\pi}} \int_0^{\infty} \exp\left[-\lambda(\sqrt{2}\sigma u - \mu - \lambda\sigma^2 + x)\right] \exp\left[-\left(\frac{x - (\sqrt{2}\sigma u - \mu - \lambda\sigma^2 + x) - \mu}{\sqrt{2}\sigma}\right)^2\right] dt, \quad (\text{A8})$$

$$= \frac{\lambda}{\sqrt{\pi}} \int_{\frac{\mu + \lambda\sigma^2 - x}{\sqrt{2}\sigma}}^{\infty} \exp\left[\lambda\mu - \lambda x + \frac{\lambda^2\sigma^2}{2}\right] \exp[-u^2] du. \quad (\text{A9})$$

$$= \frac{\lambda}{\sqrt{\pi}} \exp\left[\lambda\mu - \lambda x + \frac{\lambda^2\sigma^2}{2}\right] \int_{\frac{\mu + \lambda\sigma^2 - x}{\sqrt{2}\sigma}}^{\infty} \exp[-u^2] du. \quad (\text{A10})$$

The integral is now in the form of the complementary error function, $\int_t^{\infty} \exp[-u^2] du = \frac{\sqrt{\pi}}{2} \text{erfc}(t)$,

$$h(x; \mu, \sigma, \lambda) = \frac{\lambda}{\sqrt{\pi}} \exp\left[\lambda\mu - \lambda x + \frac{\lambda^2\sigma^2}{2}\right] \frac{\sqrt{\pi}}{2} \text{erfc}(t), \quad t = \frac{\mu + \lambda\sigma^2 - x}{\sqrt{2}\sigma} \quad (\text{A11})$$

$$= \frac{\lambda}{2} \exp\left[\frac{\lambda}{2}(2\mu + \lambda\sigma^2 - 2x)\right] \text{erfc}\left[\frac{\mu + \lambda\sigma^2 - x}{\sqrt{2}\sigma}\right]. \quad (\text{A12})$$

This the desired result, an exponentially modified Gaussian.

Appendix B: Common cases of Equation 27

In this Appendix we explicitly write out specific cases of Equation 27:

1. An IRF with one exponential decay $i \in \{1\}$ and two exponential decays in material response $j \in \{\alpha, \beta\}$
2. An IRF with two exponential decays $i \in \{1, 2\}$ and two exponential decays in material response $j \in \{\alpha, \beta\}$

1. One exponential decay in IRF and two decays in material response

Consider the case of an IRF which has one exponential decay, $i \in \{1\}$ and a material response with two exponential decays, $j \in \{\alpha, \beta\}$.

$$\mathcal{M}_{\{1\},\{\alpha,\beta\}}(x) = h_1(x) \left(\frac{a_\alpha \lambda_\alpha}{\lambda_\alpha - \lambda_1} + \frac{a_\beta \lambda_\beta}{\lambda_\beta - \lambda_1} \right) + a_1 \lambda_1 \left\{ \frac{h_\alpha(x)}{\lambda_1 - \lambda_\alpha} + \frac{h_\beta(x)}{\lambda_1 - \lambda_\beta} \right\} \quad (\text{B1})$$

$$h_1(x) = \frac{\lambda_1}{2} \exp \left[\frac{\lambda_1}{2} (2\mu + \lambda_1 \sigma^2 - 2x) \right] \operatorname{erfc} \left[\frac{\mu + \lambda_1 \sigma^2 - x}{\sqrt{2}\sigma} \right] \quad (\text{B2})$$

$$h_\alpha(x) = \frac{\lambda_\alpha}{2} \exp \left[\frac{\lambda_\alpha}{2} (2\mu + \lambda_\alpha \sigma^2 - 2x) \right] \operatorname{erfc} \left[\frac{\mu + \lambda_\alpha \sigma^2 - x}{\sqrt{2}\sigma} \right] \quad (\text{B3})$$

$$h_\beta(x) = \frac{\lambda_\beta}{2} \exp \left[\frac{\lambda_\beta}{2} (2\mu + \lambda_\beta \sigma^2 - 2x) \right] \operatorname{erfc} \left[\frac{\mu + \lambda_\beta \sigma^2 - x}{\sqrt{2}\sigma} \right] \quad (\text{B4})$$

First one would fit the measured IRF using the parameters $\{\sigma, \mu, a_1, \lambda_1\}$. Then these parameters would be held constant and the full response would be fit using the parameters $\{a_\alpha, a_\beta, \lambda_\alpha, \lambda_\beta\}$.

2. Two exponential decays in both IRF and material response

Consider the case of an IRF which has two exponential decays, $i \in \{1, 2\}$ and a material response also with two exponential decays, $j \in \{\alpha, \beta\}$.

$$\begin{aligned} \mathcal{M}_{\{1,2\},\{\alpha,\beta\}}(x) = & + h_1(x) \left(\frac{a_\alpha \lambda_\alpha}{\lambda_\alpha - \lambda_1} + \frac{a_\beta \lambda_\beta}{\lambda_\beta - \lambda_1} \right) + h_2(x) \left(\frac{a_\alpha \lambda_\alpha}{\lambda_\alpha - \lambda_2} + \frac{a_\beta \lambda_\beta}{\lambda_\beta - \lambda_2} \right) \\ & + h_\alpha(x) \left(\frac{a_1 \lambda_1}{\lambda_1 - \lambda_\alpha} + \frac{a_2 \lambda_2}{\lambda_2 - \lambda_\alpha} \right) + h_\beta(x) \left(\frac{a_1 \lambda_1}{\lambda_1 - \lambda_\beta} + \frac{a_2 \lambda_2}{\lambda_2 - \lambda_\beta} \right) \end{aligned} \quad (\text{B5})$$

$$h_1(x) = \frac{\lambda_1}{2} \exp \left[\frac{\lambda_1}{2} (2\mu + \lambda_1 \sigma^2 - 2x) \right] \operatorname{erfc} \left[\frac{\mu + \lambda_1 \sigma^2 - x}{\sqrt{2}\sigma} \right] \quad (\text{B6})$$

$$h_2(x) = \frac{\lambda_2}{2} \exp \left[\frac{\lambda_2}{2} (2\mu + \lambda_2 \sigma^2 - 2x) \right] \operatorname{erfc} \left[\frac{\mu + \lambda_2 \sigma^2 - x}{\sqrt{2}\sigma} \right] \quad (\text{B7})$$

$$h_\alpha(x) = \frac{\lambda_\alpha}{2} \exp \left[\frac{\lambda_\alpha}{2} (2\mu + \lambda_\alpha \sigma^2 - 2x) \right] \operatorname{erfc} \left[\frac{\mu + \lambda_\alpha \sigma^2 - x}{\sqrt{2}\sigma} \right] \quad (\text{B8})$$

$$h_\beta(x) = \frac{\lambda_\beta}{2} \exp \left[\frac{\lambda_\beta}{2} (2\mu + \lambda_\beta \sigma^2 - 2x) \right] \operatorname{erfc} \left[\frac{\mu + \lambda_\beta \sigma^2 - x}{\sqrt{2}\sigma} \right] \quad (\text{B9})$$

First one would fit the measured IRF using the parameters $\{\sigma, \mu, a_1, a_2, \lambda_1, \lambda_2\}$. Then these parameters would be held constant and the full response would be fit using the parameters $\{a_\alpha, a_\beta, \lambda_\alpha, \lambda_\beta\}$.

- [1] Y. Fu, M. T. Rea, J. Chen, D. J. Morrow, M. P. Hautzinger, Y. Zhao, D. Pan, L. H. Manger, J. C. Wright, R. H. Goldsmith, and S. Jin, Selective stabilization and photophysical properties of metastable perovskite polymorphs of CsPbI₃ in thin films, *Chem. Mater.* **29**, 8385 (2017).
- [2] R. H. Goldsmith and W. E. Moerner, Watching conformational- and photodynamics of single fluorescent proteins in solution, *Nat. Chem.* **2**, 179 (2010).
- [3] D. Elson, J. Requejo-Isidro, I. Munro, F. Reavell, J. Siegel, K. Suhling, P. Tadrous, R. Benninger, P. Lanihan, J. McGinty, C. Talbot, B. Treanor, S. Webb, A. Sandison, A. Wallace, D. Davis, J. Lever, M. Neil, D. Phillips, G. Stamp, and P. French, Time-domain fluorescence lifetime imaging applied to biological tissue, *Photochem. Photobiol. Sci.* **3**, 795 (2004).
- [4] P. I. Bastiaens and A. Squire, Fluorescence lifetime imaging microscopy: spatial resolution of biochemical processes in the cell, *Trends Cell Biol.* **9**, 48 (1999).
- [5] D. Gorpas, J. Phipps, J. Bec, D. Ma, S. Dochow, D. Yankelevich, J. Sorger, J. Popp, A. Bewley, R. Gandour-Edwards, L. Marcu, and D. G. Farwell, Autofluorescence lifetime augmented reality as a means for real-time robotic surgery guidance in human patients, *Sci. Rep.* **9**, 1187 (2019).
- [6] D. Comelli, C. D'Andrea, G. Valentini, R. Cubeddu, C. Colombo, and L. Toniolo, Fluorescence lifetime imaging and spectroscopy as tools for nondestructive analysis of works of art, *Appl. Opt.* **43**, 2175 (2004).
- [7] W. Becker, Fluorescence lifetime imaging - techniques and applications, *J. Microsc.* **247**, 119 (2012).
- [8] S. C. Warren, A. Margineanu, D. Alibhai, D. J. Kelly, C. Talbot, Y. Alexandrov, I. Munro, M. Katan, C. Dunsby, and P. M. W. French, Rapid global fitting of large fluorescence lifetime imaging microscopy datasets, *PLoS ONE* **8**, e70687 (2013).
- [9] M. S. Jeansonne and J. P. Foley, Review of the exponentially modified gaussian (EMG) function since 1983, *J. Chromatogr. Sci.* **29**, 258 (1991).
- [10] Y. Kalambet, Y. Kozmin, K. Mikhailova, I. Nagaev, and P. Tikhonov, Reconstruction of chromatographic peaks using the exponentially modified gaussian function, *J. Chemometrics* **25**, 352 (2011).
- [11] S. Purushothaman, S. A. S. Andrés, J. Bergmann, T. Dickel, J. Ebert, H. Geissel, C. Hornung, W. Plaf, C. Rappold, C. Scheidenberger, Y. Tanaka, and M. Yavor, Hyper-EMG: A new probability distribution function composed of exponentially modified gaussian distributions to analyze asymmetric peak shapes in high-resolution time-of-flight mass spectrometry, *Int. J. Mass. Spectrom.* **421**, 245 (2017).
- [12] A. Golubev, Exponentially modified peak functions in biomedical sciences and related disciplines, *Comput. Math. Methods Med.* **2017**, 7925106 (2017).
- [13] D. Matzke and E.-J. Wagenmakers, Psychological interpretation of the ex-gaussian and shifted wald parameters: A diffusion model analysis, *Psychon. Bull. Rev.* **16**, 798 (2009).
- [14] D. Pan, Y. Fu, N. Spitha, Y. Zhao, C. R. Roy, D. J. Morrow, D. D. Kohler, J. C. Wright, and S. Jin, Deterministic fabrication of arbitrary vertical heterostructures of two-dimensional ruddlesden–popper halide perovskites, *Nat. Nanotechnol.* **16**, 159 (2020).
- [15] G. A. Elbaz, D. B. Straus, O. E. Semonin, T. D. Hull, D. W. Paley, P. Kim, J. S. Owen, C. R. Kagan, and X. Roy, Unbalanced hole and electron diffusion in lead bromide perovskites, *Nano Lett.* **17**, 1727 (2017).
- [16] D. J. Lockwood and Z. R. Wasilewski, Optical phonons in Al_xGa_{1-x}As: Raman spectroscopy, *Phys. Rev. B* **70**, 155202 (2004).
- [17] H. Ardekani, R. Younts, Y. Yu, L. Cao, and K. Gundogdu, Reversible photoluminescence tuning by defect passivation via laser irradiation on aged monolayer MoS₂, *ACS Appl. Mater. Interfaces* **11**, 38240 (2019).
- [18] W. S. Yoo, K. Kang, G. Murai, and M. Yoshimoto, Temperature dependence of photoluminescence spectra from crystalline silicon, *ECS J. Solid State Sci. Technol.* **4**, P456 (2015).
- [19] M. R. Zaghoul and A. N. Ali, Algorithm 916: Computing the faddeyeva and voigt functions, *ACM Trans. Math. Softw.* **38**, 1 (2011).
- [20] S. M. Abrarov and B. M. Quine, A rational approximation of the dawson's integral for efficient computation of the complex error function, *Appl. Math* **321**, 526 (2018).
- [21] M. Van Den Zegel, N. Boens, D. Daems, and F. De Schryver, Possibilities and limitations of the time-correlated single photon counting technique: a comparative study of correction methods for the wavelength dependence of the instrument response function, *Chem. Phys.* **101**, 311 (1986).
- [22] Y. Li, S. Natakorn, Y. Chen, M. Safar, M. Cunningham, J. Tian, and D. D.-U. Li, Investigations on average fluorescence lifetimes for visualizing multi-exponential decays, *Front. Phys.* **8**, 447 (2020).
- [23] N. Spitha, D. D. Kohler, M. P. Hautzinger, J. Li, S. Jin, and J. C. Wright, Discerning between exciton and free-carrier behaviors in ruddlesden–popper perovskite quantum wells through kinetic modeling of photoluminescence dynamics, *J. Phys. Chem. C* **124**, 17430 (2020).
- [24] L. H. Manger, M. B. Rowley, Y. Fu, A. K. Foote, M. T. Rea, S. L. Wood, S. Jin, J. C. Wright, and R. H. Goldsmith, Global analysis of perovskite photophysics reveals importance of geminate pathways, *J. Phys. Chem. C* **121**, 1062 (2017).
- [25] R. G. W. Brown, K. D. Ridley, and J. G. Rarity, Characterization of silicon avalanche photodiodes for photon correlation measurements 1: Passive quenching, *Appl. Opt.* **25**, 4122 (1986).
- [26] A. W. Ziarkash, S. K. Joshi, M. Stipčević, and R. Ursin, Comparative study of afterpulsing behavior and models in single photon counting avalanche photo diode detectors, *Sci. Rep.* **8**, 5076 (2018).